Synthesis of Large-Sized Single-Crystal Hexagonal Boron Nitride Domains on Nickel Foils by Ion Beam Sputtering Deposition

Haolin Wang, Xingwang Zhang, Heng Liu, Zhigang Yin, Junhua Meng, Jing Xia, Xiang-Min Meng, Jinliang Wu, and Jingbi You*

Atomically thin 2D materials have attracted significant attention because of their unique structures, interesting physical properties, and potential applications. Among the family of 2D materials, hexagonal boron nitride (h-BN), consisting of alternating boron and nitrogen atoms arranged in an sp^2-bonded network within each layer, occupies a special position, being an insulator isostructural to graphene.[1–3] Due to its close lattice matching with graphene, as well as atomically flat and dangling-bond-free surface, h-BN has proven to be an ideal dielectric substrate of graphene for improved device quality.[4–7] For example, an order of magnitude improvement in carrier mobility,[4] micrometer scale ballistic transport[8] and quantum Hall effect[9] have been observed in the graphene/h-BN heterostructures. Additionally, h-BN also has a wide range of applications in mechanical and thermal coat ings, deep ultraviolet (DUV) optoelectronic devices, and transparent electronics. The synthesis of large-scale high-quality h-BN layers with a low density of defects is strongly desired to meet these applications.

Similar to graphene, h-BN flakes can be obtained by mechanical or liquid-phase exfoliation from h-BN single crystals, but the limited flake size makes them less suitable for large-scale applications.[1,10] Chemical vapor deposition (CVD) is regarded as the most promising method, and it has been reported to synthesize h-BN on a range of transition catalyst metals, including Cu,[2,5,6,11,12] Pt,[13–15] and Ni[3,16,17] polycrystalline foils in atmospheric pressure or low-pressure CVD, as well as on Ru,[18] Rh,[19] and Pt[20] single crystals in ultrahigh vacuum CVD. In the earlier reports, the sizes of h-BN domains were limited to ≈1 μm on both Cu and Pt foils.[11–13] Recently, it has been found that substrates have great influence on the h-BN film growth.[21–24] Tay et al. synthesized hexagonal-shape h-BN domains with an area of 35 μm^2 using highly smoothened electropolished Cu substrates by atmospheric pressure CVD,[21] while Wang et al. demonstrated 20 μm triangular-shaped h-BN domains by extended thermal annealing of Cu foils under low-pressure CVD conditions.[22] Very recently, single-crystal h-BN domains with lateral sizes of more than 100 μm were synthesized by rationally designing the Cu–Ni alloy substrate[23] or via an admixture of Si to Fe catalyst substrates.[24] However, the individual h-BN domains are only >25 μm in average lateral size for the continuous film. Moreover, the CVD process needs to utilize rather unconventional boron-containing precursors, and these compounds are not only very expensive, but also highly toxic, unstable, or pyrophoric in nature.[25] To avoid these problems, ion beam sputtering deposition (IBSD) has been firstly employed for synthesizing high quality h-BN in our previous work, in which h-BN domains with a size up to 5 μm on Cu foils have been obtained.[26]

In this work, we report the successful synthesis of large-sized single-crystal h-BN domains on polycrystalline Ni foils by IBSD. The nucleation density of h-BN can be dramatically decreased by the in situ pretreatment of Ni substrates, as well as by elaborately controlling the growth temperature and the ion beam density. The growth strategies and characterization of large-sized h-BN domains with the length of side up to 100 μm are discussed. Furthermore, the synthesized h-BN films were also used to demonstrate applicability for detecting DUV photons. These results present a promising route toward large-scale high-quality h-BN layers for electronic applications.

We have recently developed a method of synthesizing h-BN domains with a lateral size up to 5 μm on Cu foils by using IBSD.[26] In the present work, using the same IBSD technique, we adopted commercial Ni foils of 99.5% purity as substrates for the preparation of large-sized h-BN domains. Prior to the IBSD growth, the Ni foils were in situ etched by an assisting ion source, followed by annealing at 1000 °C for 10 min, and then boron and nitrogen species were sputtered from an h-BN target by 1.0 keV Ar ions from the primary ion source. During the sputtering process, the chamber was kept at a constant pressure of 3×10^{-2} Pa, and the typical growth temperature was 1000 °C. After growth, the h-BN films on Ni foils were cooled down to room temperature in Ar atmosphere and then transferred onto different substrates for characterization. The schematic diagram of the IBSD system with two independent ion sources is illustrated in **Figure 1**, and the experimental details are given in the Experimental Section.

According to recent reports, the surface morphology of substrates plays an important role to limit the initial density of nuclei in order to grow large-sized single-crystal h-BN

H. L. Wang, Prof. X. W. Zhang, H. Liu,
Dr. Z. G. Yin, J. H. Meng, J. L. Wu, Prof. J. B. You
Key Lab of Semiconductor Materials Science
Institute of Semiconductors
Chinese Academy of Sciences
Beijing 100083, P. R. China
E-mail: xwzhang@semi.ac.cn

J. Xia, Prof. X.-M. Meng
Key Lab of Photochemical Conversion
and Optoelectronic Materials
Technical Institute of Physics and Chemistry
Chinese Academy of Sciences
Beijing 100190, P. R. China

DOI: 10.1002/adma.201504042

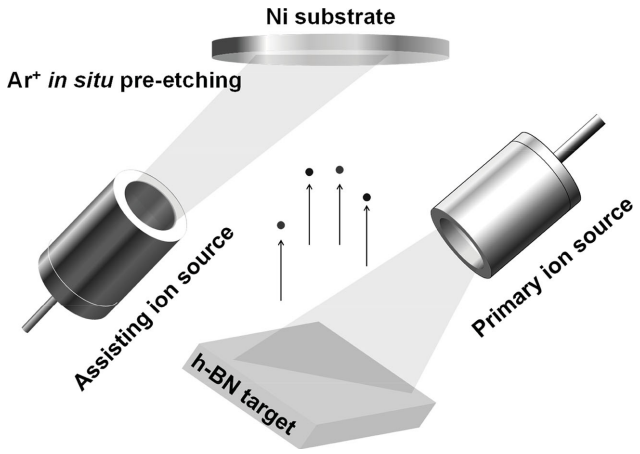

Figure 1. Schematic diagram of the IBSD system with two independent Kaufmann ion sources. The primary ion source was used to sputter h-BN target for growing h-BN, while the assisting ion source was used to pre-etch Ni substrates prior to the growth.

domains.[21,22] To reduce the surface roughness and remove attached impurities, the Ni substrates were in situ etched by an assisting ion source before the IBSD growth. As shown in Figure S1 (Supporting Information), the surface of Ni substrates is much smoother, and some large particles have vanished after ion beam etching. The root-mean-square (RMS) roughness, R_q of 7.5 nm, was obviously reduced as compared to an as-purchased Ni foil, R_q of 36 nm, scanned within an area of 10×10 μm^2. The IBSD growth of h-BN was carried out on both etched and unetched Ni foils under the same conditions and parameters. **Figure 2**a,b shows the scanning electron microscopy (SEM) images of h-BN domains grown at 1000 °C for 10 min with an ion beam density of 0.15 mA cm^{-2} on the etched and unetched substrates, respectively. Most h-BN domains on the unetched substrate exhibit triangular shapes due to the asymmetric N and B-terminated edge energies,[27] and the size of h-BN domains ranges approximately from 20 to 25 μm, which is 4–5 times larger than those on Cu foils grown with the same method (Figure S2, Supporting Information). It is interesting to note the contrasting difference between the densities of h-BN domain on different Ni surfaces. As a result, larger triangular h-BN domains are observed on the etched Ni substrate with a lateral size of 80 μm, which is an order of magnitude larger than the most h-BN domains by CVD. The edges of some domains are sawtoothed, with each tooth having edge length of ≈10 μm. Recent theory calculations indicate that diffusion instabilities result in sawtoothed edge geometries,[28] and the similar morphology has also been observed in the single-crystal h-BN domains by CVD via Si-doped Fe catalysts.[24] From previous reports on the influence of substrate surface morphology on the growth of h-BN or graphene, it is known that the rough surfaces or presence of impurities and grain boundaries are likely to act as nucleation seeds, leading to an enhanced rate of nucleation.[21,29,30] Herein, the pretreatment of Ni substrate by ion beam etching is considered to be one of the critical factors for the growth of large-sized h-BN domains.

It was previously reported that direct visualization of graphene or h-BN domains on Cu surface can be realized by oxidizing uncovered Cu surface via annealing in air.[22] Here we apply this technique to h-BN domains on Ni surface, as shown in Figure 2c, made visible by oxidizing the unprotected Ni surface by heat treatment in air at 500 °C for 15 min. Triangular-shaped h-BN domains can be clearly identified as darker region in the image, and this well-defined shape is an indication of single-crystal h-BN domain as observed in the corresponding SEM image. Figure 2d shows an optical microscope image of transferred h-BN domains on SiO_2/Si, and the uniform contrast indicates the macroscopic uniformity. By increasing the growth time to 25 min, the growing h-BN domains might contact with

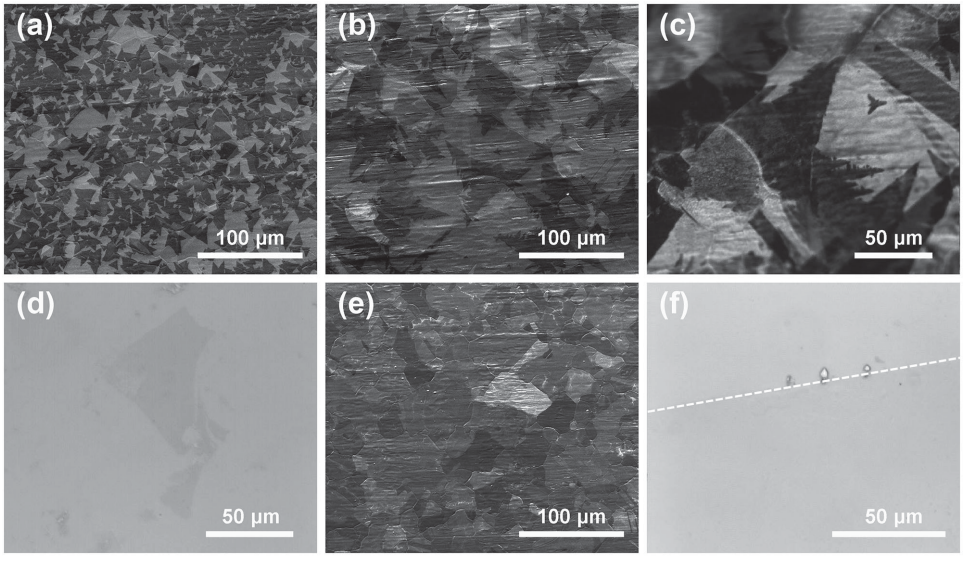

Figure 2. Morphology of h-BN domains. SEM images of h-BN domains deposited at 1000 °C with an ion beam density of 0.15 mA cm^{-2} for 10 min on a) unetched and b) etched Ni foils. c) Optical image of h-BN domains grown on Ni surface with oxidation treatment in air. d) Optical microscopy image of an h-BN domain transferred onto a 300 nm SiO_2/Si substrate. e) SEM image of a continuous h-BN film deposited under the same condition for 25 min. f) Optical image of the h-BN film on a 300 nm SiO_2/Si. White dotted line indicates the border between h-BN and SiO_2 in (f).

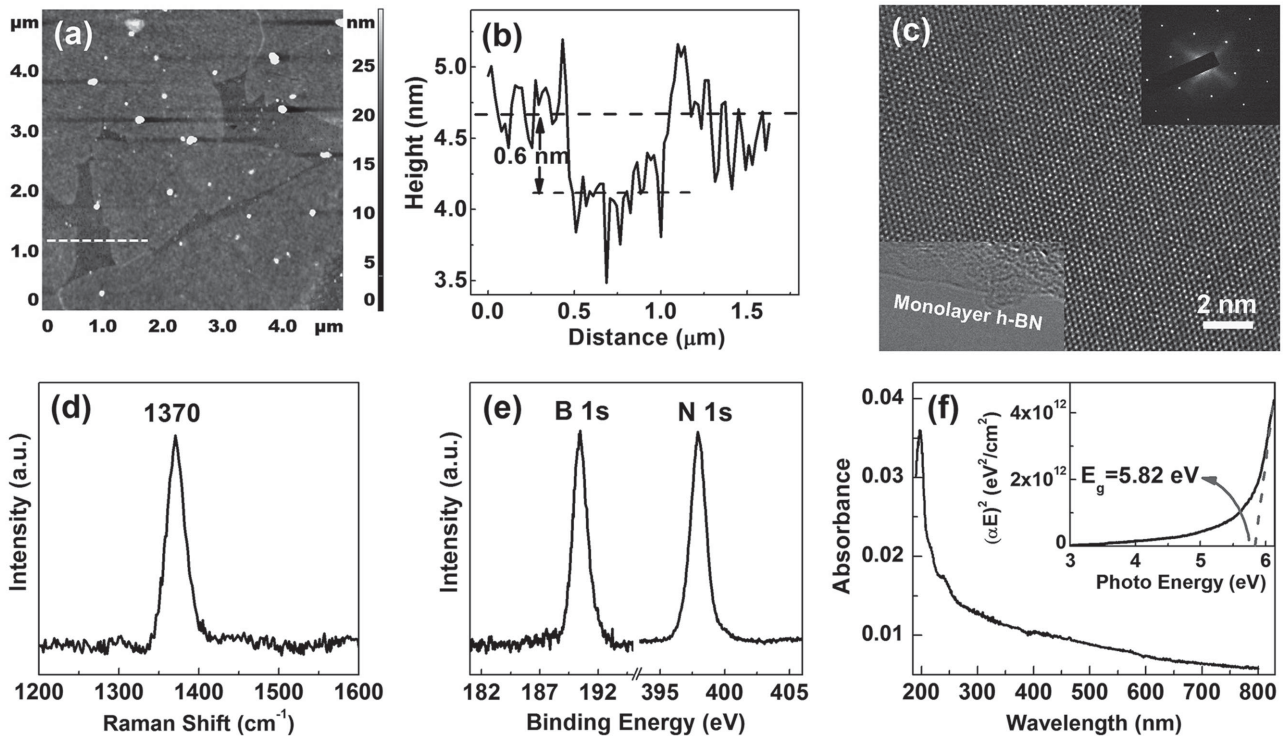

Figure 3. Characterization of h-BN domains. a) AFM image of h-BN domains transferred onto a 300 nm SiO_2/Si substrate. b) The height profile along the white line drawn in (a), showing a thickness of 0.6 nm. c) Top-view HRTEM image of h-BN domains, with the corresponding hexagonal electron diffraction pattern (top right inset) and edge analysis, confirming the single layer nature of the film (bottom left inset). d) Raman spectrum of h-BN domains on a SiO_2/Si substrate. e) XPS core-level spectra of B 1s and N 1s. f) UV–vis spectrum of h-BN film transferred on a transparent quartz substrate. The inset shows optical band gap (5.82 eV) analysis of h-BN from (f).

the adjacent domains and form a continuous film as shown in Figure 2e. Unlike h-BN on Cu,[26] the uniform h-BN film without visible grain boundaries was formed on the Ni foil, and the different contrasts in Figure 2e are attributed to the polycrystalline nature of the underlying Ni foil. In addition, it is difficult to distinguish between monolayer h-BN and SiO_2 by optical microscopy because of the small optical contrast between them.[31] Some impurities at the edge of the film help to recognize the h-BN/SiO_2 border,[11] as indicated by the white dotted line in Figure 2f.

Figure 3a shows the atomic force microscopy (AFM) image of the h-BN domains transferred onto a SiO_2/Si substrate, and the sharp edges of h-BN domains can be observed clearly. From the step height profile at the domain edge (Figure 3b), the thickness of the h-BN domain is estimated to be about 0.6 nm, consistent with the monolayer h-BN.[32] The slight increase in AFM thickness measurement for a monolayer h-BN is likely due to the chemical contrast between the h-BN domain and the SiO_2 substrate, as reported previously.[21,33,34] For a more reliable measurement of h-BN layer, transmission electron microscopy (TEM) was utilized. Figure 3c shows a representative high-resolution TEM (HRTEM) image recorded at an h-BN domain transferred onto a Cu grid, as well as a cross-sectional TEM image taken at the folded edge (inset of Figure 3c). A line shape contrast confirms the single layer feature of the as-grown h-BN. The selected area electron diffraction (SAED) pattern presented in the inset of Figure 3c shows a set of characteristic six-fold symmetric spots, indicating that the h-BN domain is well crystallized. The SAED patterns recorded at different locations on a large h-BN domain, all have identical orientation (Figure S3, Supporting Information), confirming the single-crystal nature of h-BN domains.[22,24] Moreover, it was reported that the Ni substrates usually led to multi-layered growth of h-BN for the atmospheric pressure or low-pressure CVD technique,[3,16,17] while the monolayer h-BN was grown in ultrahigh vacuum CVD.[35] The growth mechanism of h-BN on Ni is still unclear, and it is neither surface-limited nor dominated by segregation and precipitation of B and N. We propose that two mechanisms, surface-mediated reaction and gas phase nucleation/growth, are responsible for the growth of h-BN on Ni, depending on the feeding rate of precursors (or the growth rate). For atmospheric pressure and low-pressure CVD techniques, the higher concentration of precursors leads to the gas phase nucleation and growth on the first monolayer, promoting the formation of the multilayer structure. In the cases of ultrahigh vacuum CVD and IBSD, the gas phase nucleation and growth can be ignored due to the much lower concentration of precursors. Therefore, after a full monolayer is formed, the growth rate of h-BN significantly drops, leading to predominately monolayer h-BN. Further studies are underway to elucidate the growth mechanisms of h-BN on Ni.

To further confirm the existence and quality of monolayer h-BN, the h-BN domains were also characterized by Raman spectroscopy, X-ray photoemission spectroscopy (XPS), and UV–vis absorption spectroscopy. Figure 3d shows a typical Raman spectrum taken from the transferred h-BN domain, exhibiting

the characteristic peak at about 1370 cm^{-1}, which is attributed to the in-plane ring vibration of monolayer h-BN.[36] The full width at half maximum of the peak is ≈24 cm^{-1}, again suggesting the high crystallinity. As shown in Figure 3e, the B 1s and N 1s core-level peaks are centered at 190.1 and 398.2 eV, respectively, consistent with the previously reported values.[3,17,21,22] The B/N ratio from our XPS survey is calculated to be 0.98, indicative of the predominant B–N bond in the sample. Figure 3f shows an UV–vis absorption spectrum of the h-BN film transferred onto a transparent quartz substrate, and a strong peak is observed at ≈200 nm in the absorption spectrum, characteristics of 2D h-BN. By using the formula for a direct band semiconductor,[37] the optical band gap of h-BN is determined to be 5.82 eV as shown in the inset of Figure 3f, which is very close to the theoretical calculations and the previous experimental data.[17,38,39] The measured band gap also suggests the as-grown h-BN film to be highly transparent and electrically insulating.

As demonstrated above, the surface morphology of substrate is one of the most important factors to limit the nucleation density, thus the size of h-BN domains. Besides, the feeding rate of precursor is another critical factor to determine the nucleation density for the CVD-grown h-BN.[32,40] For the IBSD process, we expect that the growth rate, which is related to the ion beam density of primary source and the growth temperature in this work, plays a similar critical role. Therefore, systematic studies were carried out to find out the optimum conditions for the preparation of the large-sized h-BN domains. **Figure 4**a–d shows the SEM images of the h-BN domains prepared on the Ni foils at a fixed temperature of 1000 °C with various ion beam densities. The growth time was 16, 8, 5, and 4 min for the ion beam density of 0.1, 0.2, 0.3, and 0.4 mA cm^{-2}, respectively. To avoid the formation of a continuous h-BN film, the shorter growth time was chosen for the higher ion beam density. Obviously, the lower ion beam density leads to a significant increase in the domain size, while the h-BN domain shape still remains the typical triangles. To clearly demonstrate the effects of ion beam density on the h-BN growth, both the maximum lateral size and the density of h-BN domains as a function of the ion beam density are shown in Figure 4e. The maximum lateral size of h-BN domains increased from 25 to 110 μm with the density of domains decreasing from 2770 to 550 mm^{-2}, when the ion beam density reduced from 0.4 to 0.1 mA cm^{-2}.

Next we show the effects of growth temperature on the h-BN domain density/size, with the ion beam density fixed at 0.1 mA cm^{-2}. **Figure 5**a–d shows the SEM images of h-BN prepared at the temperature of 600, 800, 900, and 1100 °C for 10 min, respectively. It can be seen that the h-BN domains grown at 800 and 900 °C exhibit much smaller sizes of 20–30 μm, as well as irregular shapes instead of the typical triangles at 1000 °C (Figure 5b,c). When the growth temperature was decreased to 600 °C, the domain structure could not be distinguished anymore, as shown in Figure 5a. A zoom-in view of the sample surface (inset of Figure 5a) shows that a continuous film with uniformly distributed nanoparticles was formed on substrate. Further characterizations by XPS and Raman spectroscopy (Figure S4, Supporting Information) reveal that the film grown at 600 °C consists of an amorphous BN. On the other hand, because the higher temperature leads to more effective desorption of the active species, there is almost

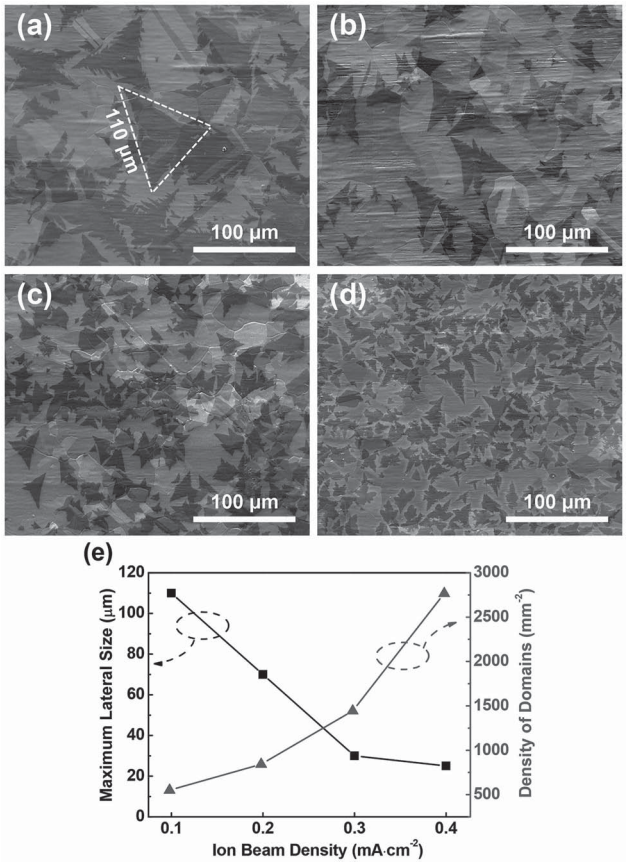

Figure 4. SEM images of the h-BN domains prepared on the Ni foils at 1000 °C with ion beam densities of a) 0.1 mA cm^{-2} for 16 min, b) 0.2 mA cm^{-2} for 8 min, c) 0.3 mA cm^{-2} for 5 min, and d) 0.4 mA cm^{-2} for 4 min. The shorter growth time was chosen for the higher ion beam density to avoid the formation of a continuous h-BN film. e) The maximum lateral size and the density of h-BN domains as a function of the ion beam density.

no h-BN domain or film for the sample grown at 1100 °C for 10 min (Figure 5d), except for occasionally observed triangular h-BN nuclei (inset of Figure 5d). Even the growth process was prolonged to 25 min, there are still only some sparse h-BN nuclei were obtained (Figure S5a, Supporting Information). To compensate fast desorption of the species and prepare large-sized h-BN domains at such high temperature, an additional sample was prepared at 1100 °C for 15 min with a relatively high ion beam density of 0.2 mA cm^{-2}. In this case, triangular-shaped h-BN domains with the maximum lateral size of ≈100 μm were observed, as shown in Figure S5b (Supporting Information). These results indicate that high temperature is favorable for growing large-sized h-BN domains, however, a too high temperature always inhibits the nucleation and growth of h-BN due to the speeding desorption of active species.

Reducing the nucleation density is the prerequisite for growing large-sized single-crystal h-BN domains. Generally, there are many factors in determining the nucleation density of h-BN, such as substrate type and morphology, external impurities, growth rate and growth temperature. Due to the high chemical affinity of N-containing intermediate species to the Cu surface,[41] the nucleation density of h-BN on Cu foils is usually higher, resulting in h-BN domains with only several μm. In this work, the Ni foils

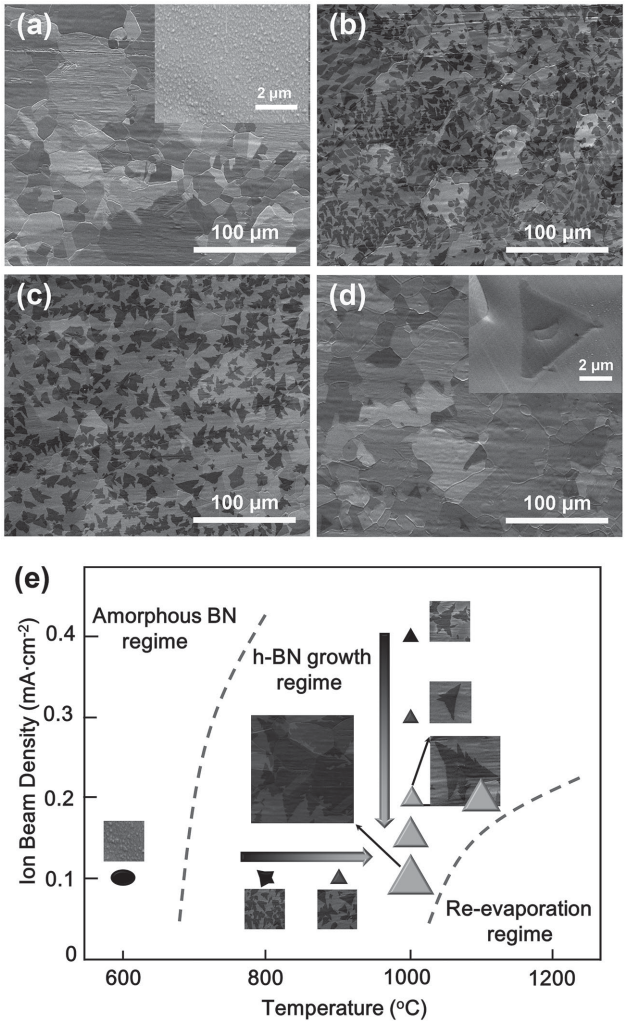

Figure 5. SEM images of the h-BN domains prepared on the Ni foils with an ion beam density of 0.1 mA cm^{-2} at a) 600, b) 800, c) 900, and d) 1100 °C for 10 min. The inset of (a) shows a zoom-in view of the sample surface. The inset of (d) shows the enlarged image of one h-BN nucleus. e) Schematic drawing of the dependence of h-BN domain size on the ion beam density and the growth temperature, from which three regimes can be identified, as indicated by the red dashed lines.

were adopted as substrates, and the density of h-BN domains was significantly reduced and the size of h-BN domain (20 μm) was 4–5 times larger than that of h-BN on Cu.[26] On the other hand, defects on the substrate, such as impurities, dislocation, and surface irregularities normally serve as nucleation centers. To reduce substrate roughness and remove impurities, the Ni foil was in situ etched by the assisting ion beam for 5 min prior to h-BN growth. As a result, the increased Gibbs free energy barrier and enhanced surface diffusivity due to the smoothened surface suppress the nucleation of h-BN,[21,42] allowing for the growth of large-sized domains (80 μm). Beside substrate defects, further optimization of the process gives us the opportunity of achieving larger domain sizes. As shown in Figure 5e, both the higher temperature and the lower density of ion beam lead to a larger size of h-BN domains. The lower density of ion beam reduces the feeding rate of sputtered atoms or clusters, while the higher growth temperature promotes desorption and surface diffusion of active species. Both of these contribute to diluting the concentrations of active species on the Ni surface and therefore the decrease of the h-BN nucleation density, enabling the growth of large-sized h-BN domains during the extended growth time. Under the optimized conditions, the size of h-BN domains increases to more than 100 μm. However, too high temperature (>1100 °C) or too low density of ion beam (<0.1 mA cm^{-2}) impedes the rate of h-BN nucleation due to the competition between the processes of adatom capture, surface diffusion, and desorption. Consequently, h-BN cannot be grown in this regime, which is labeled as "re-evaporation regime" in Figure 5e. On the other hand, too low temperatures (600 °C) suppress the surface diffusion of active species, leading to the formation of an amorphous BN film, labeled as "amorphous BN regime". Moreover, our previous results indicate that the sizes of h-BN domains on Cu foils were significantly increased by introducing H_2 during the growth process.[26] Nevertheless, H_2 has almost no influence on the size of h-BN domains grown on Ni foils (Figure S6, Supporting Information).

Due to its direct band gap of 5.90 eV, h-BN could be a promising candidate for DUV photodetector.[38,43] In view of this, we fabricated a prototype photodetector based on the h-BN monolayer and demonstrated its performance in detecting UV photons. Briefly, the as-grown monolayer h-BN films were transferred onto a 300 nm SiO_2/Si substrate, and then two Au strip electrodes separated by 0.5 mm were deposited on the top of the 1 mm wide h-BN monolayer through a shadow mask by electron beam evaporation. Finally, the as-fabricated devices were annealed under the N_2 atmosphere at 400 °C for 30 min to improve the contact. Electrical measurements were carried out in the dark and in the presence of a DUV deuterium lamp (inset of **Figure 6**a). As shown in Figure 6, the dark current is the order of 10^{-10} amp at 3 V, indicating the electrically insulating character of the h-BN film. The current is significantly increased by three orders of magnitude when the device is illuminated. Only the noise current was collected for the reference detector with the same geometry but without h-BN layer (Figure S7, Supporting Information), excluding the possibility that the observed photocurrent is generated from the underlying SiO_2 or the Au electrodes. A symmetric diode characteristic implies a contact barrier formed between the Au electrodes and h-BN. Figure 6b shows the current as a function of time at a bias voltage of 5 V when the deuterium lamp is switched on and off periodically. The device shows a low off-state current of 1.5 nA and a high on-state current of 1.7 μA, giving a high on/off ratio of 10^3. After multiple illumination cycles, the photocurrent still responded in a similar fashion to the illumination, demonstrating good reproducibility and high robustness.

In conclusion, we have successfully grown large single-crystal h-BN domains with a lateral size up to 100 μm on Ni foils using IBSD. A brief in situ pre-etching of Ni substrate by the assisting ion beam can effectively eliminate surface irregularities and remove impurities, resulting in a significant reduction in nucleation density. The nucleation density can be further decreased by reducing the concentrations of active species on the Ni surface through elaborately controlling the growth temperature and the ion beam density, enabling the growth of large-sized h-BN domains. In addition, the DUV photoresponse of h-BN was also demonstrated, suggesting that h-BN is a

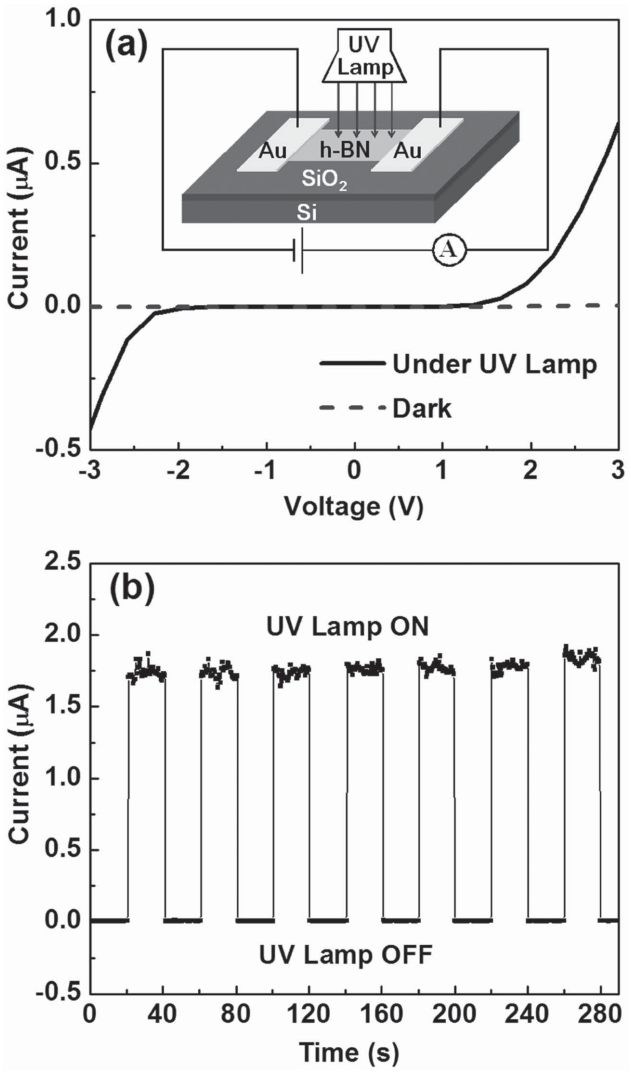

Figure 6. a) *I–V* characteristics of the device in the dark and under a DUV deuterium lamp illumination. The inset shows the schematic view of the device operation. b) Time-dependent photocurrent of the detector at a bias voltage of 5 V.

potential material for photodetection applications. This controllable, scalable and benign method is a promising technique for growing high-quality h-BN layers and opens up a fascinating perspective for high-performance graphene/h-BN electronics.

Experimental Section

Growth of h-BN by IBSD: The h-BN layers were prepared on the Ni foils in an IBSD chamber equipped with two independent Kaufmann ion sources. The Ni foils (99.5% purity, 25 μm thickness, Alfa Aesar) were sequentially cleaned in the ultrasonic baths of acetone, ethanol, and deionized water, and then blown dried with nitrogen gas. Next, the Ni foils were placed on the sample holder at a distance of 40 cm from the h-BN target (99.0% purity, Good Fellow), and then the chamber was pumped to a base pressure (2×10^{-5} Pa). Prior to the growth, the Ni substrates were etched by an Ar ion beam (500 eV, 0.05 mA cm^{-2}) from the assisting ion source for 5 min, and followed by annealing at 1000 °C for 10 min to obtain a clean and smooth surface. During the pre-etching of Ni foils, the h-BN target was protected by a removable cover which is fixed to the end of a linear feed-through. After that, the substrate temperature was adjusted to the desired growth temperature ranging from 600 to 1100 °C, and the growth of h-BN layers was commenced by sputtering h-BN target with the Ar^+ ions (1.0 keV, 0.1–0.4 mA cm^{-2}) supplied from the primary ion source. During the growth process, the chamber was kept at a constant pressure (3×10^{-2} Pa). After the growth procedure, the primary ion source was shut down and the samples were cooled down to room temperature in pure Ar atmosphere.

Transfer: The h-BN was transferred on different substrates for characterization with the same method for graphene. The as-grown samples were spin-coated with poly(methyl methacrylate) (PMMA) (4.0% in anisole) on the surface as a supportive layer, and then the underlying Ni was etched away by $FeCl_3$ reagent. Subsequently, the PMMA/h-BN films were washed by deionized water to remove the residual reagent. The PMMA/h-BN films were then transferred to the target substrates, and the PMMA was dissolved in acetone, leaving the h-BN film for subsequent characterization.

Characterization: The morphology and structure of h-BN layers were characterized using SEM (FEI Quanta-450), AFM (NT-MDT Solver P47, tapping mode), TEM (JEOL JEM-2100F, 200 kV), and optical microscope (Olympus MX51). For TEM characterization, an ultrathin carbon film supported on a Cu grid was used. Raman spectroscopy was measured with a Renishaw inVia-Reflex spectrometer using a 532 nm laser as the excitation source. XPS measurements were carried out on an EscaLab 250Xi instrument with a monochromated Al Kα source (1486.68 eV). Optical absorption spectra of the samples were acquired by using a Varian Cary 5000 UV–vis spectrophotometer in a double-beam mode. The electrical measurements were carried out with a Keithley 2400 source measure unit. Photocurrent measurements were performed at room temperature under atmospheric conditions with the deuterium lamp emitting at 190 nm.

Supporting Information

Supporting Information is available from the Wiley Online Library or from the author.

Acknowledgements

This work was financially supported by the National Natural Science Foundation of China (Nos. 61376007 and 11274303), the National Basic Research Program of China (No. 2012CB619306), the Beijing Natural Science Foundation (No. 2142032), and the Strategic Priority Research Program on Space Science, the CAS (Grant No. XDA04020411).

Received: August 19, 2015
Revised: September 20, 2015
Published online: November 2, 2015

[1] M. Xu, T. Liang, M. Shi, H. Chen, *Chem. Rev.* **2013**, *113*, 3766.
[2] L. Song, L. J. Ci, H. Lu, P. B. Sorokin, C. H. Jin, J. Ni, A. G. Kvashnin, D. G. Kvashnin, J. Lou, B. I. Yakobson, P. M. Ajayan, *Nano Lett.* **2010**, *10*, 3209.
[3] Y. Shi, C. Hamsen, X. Jia, K. K. Kim, A. Reina, M. Hofmann, A. L. Hsu, K. Zhang, H. Li, Z.-Y. Juang, M. S. Dresselhaus, L.-J. Li, J. Kong, *Nano Lett.* **2010**, *10*, 4134.
[4] C. R. Dean, A. F. Young, I. Meric, C. Lee, L. Wang, S. Sorgenfrei, K. Watanabe, T. Taniguchi, P. Kim, K. L. Shepard, J. Hone, *Nat. Nanotechnol.* **2010**, *5*, 722.
[5] K. H. Lee, H.-J. Shin, J. Lee, I. Lee, G.-H. Kim, J.-Y. Choi, S.-W. Kim, *Nano Lett.* **2012**, *12*, 714.

[6] K. K. Kim, A. Hsu, X. Jia, S. M. Kim, Y. Shi, M. Dresselhaus, T. Palacios, J. Kong, *ACS Nano* **2012**, *6*, 8583.
[7] M. P. Levendorf, C.-J. Kim, L. Brown, P. Y. Huang, R. W. Havener, D. A. Muller, J. Park, *Nature* **2012**, *488*, 627.
[8] A. S. Mayorov, R. V. Gorbachev, S. V. Morozov, L. Britnell, R. Jalil, L. A. Ponomarenko, P. Blake, K. S. Novoselov, K. Watanabe, T. Taniguchi, A. K. Geim, *Nano Lett.* **2011**, *11*, 2396.
[9] W. Yang, G. Chen, Z. Shi, C. -C. Liu, L. Zhang, G. Xie, M. Cheng, D. Wang, R. Yang, D. Shi, K. Watanabe, T. Taniguchi, Y. Yao, Y. Zhang, G. Zhang. *Nat. Mater.* **2013**, *12*, 792.
[10] J. N. Coleman, M. Lotya, A. O'Neill, S. D. Bergin, P. J. King, U. Khan, K. Young, A. Gaucher, S. De, R. J. Smith, I. V. Shvets, S. K. Arora, G. Stanton, H.-Y. Kim, K. Lee, G. T. Kim, G. S. Duesberg, T. Hallam, J. J. Boland, J. J. Wang, J. F. Donegan, J. C. Grunlan, G. Moriarty, A. Shmeliov, R. J. Nicholls, J. M. Perkins, E. M. Grieveson, K. Theuwissen, D. W. McComb, P. D. Nellist, V. Nicolosi, *Science* **2011**, *331*, 568.
[11] K. K. Kim, A. Hsu, X. Jia, S. M. Kim, Y. Shi, M. Hofmann, D. Nezich, J. F. Rodriguez-Nieva, M. Dresselhaus, T. Palacios, J. Kong, *Nano Lett.* **2012**, *12*, 161.
[12] M. H. Khan, Z. Huang, F. Xiao, G. Casillas, Z. Chen, P. J. Molino, H. K. Liu, *Sci. Rep.* **2015**, *5*, 7743.
[13] Y. Gao, W. Ren, T. Ma, Z. Liu, Y. Zhang, W. B. Liu, L. P. Ma, X. Ma, H.-M. Cheng, *ACS Nano* **2013**, *7*, 5199.
[14] G. Kim, A.-R. Jang, H. Y. Jeong, Z. Lee, D. J. Kang, H. S. Shin, *Nano Lett.* **2013**, *13*, 1834.
[15] J.-H. Park, J. C. Park, S. J. Yun, H. Kim, D. H. Luong, S. M. Kim, S. H. Choi, W. Yang, J. Kong, K. K. Kim, Y. H. Lee, *ACS Nano* **2014**, *8*, 8520.
[16] Y.-H. Lee, K.-K. Liu, A.-Y. Lu, C.-Y. Wu, C.-T. Lin, W. Zhang, C.-Y. Su, C.-L. Hsu, T.-W. Lin, K.-H. Wei, Y. Shi, L.-J. Li, *RSC Adv.* **2012**, *2*, 111.
[17] A. Ismach, H. Chou, D. A. Ferrer, Y. Wu, S. McDonnell, H. C. Floresca, A. Covacevich, C. Pope, R. Piner, M. J. Kim, R. M. Wallace, L. Colombo, R. S. Ruoff, *ACS Nano* **2012**, *6*, 6378.
[18] P. Sutter, J. Lahiri, P. Albrecht, E. Sutter, *ACS Nano* **2011**, *5*, 7303.
[19] S. Berner, M. Corso, R. Widmer, O. Groening, R. Laskowski, P. Blaha, K. Schwarz, A. Goriachko, H. Over, S. Gsell, M. Schreck, H. Sachdev, T. Greber, J. Osterwalder, *Angew. Chem. Int. Ed.* **2007**, *46*, 5115.
[20] F. Müller, K. Stöwe, H. Sachdev, *Chem. Mater.* **2005**, *17*, 3464.
[21] R. Y. Tay, M. H. Griep, G. Mallick, S. H. Tsang, R. S. Singh, T. Tumlin, E. H. T. Teo, S. P. Karna. *Nano Lett.* **2014**, *14*, 839.
[22] L. F. Wang, B. Wu, J. S. Chen, H. T. Liu, P. A. Hu, Y. Q. Liu, *Adv. Mater.* **2014**, *26*, 1559.
[23] G. Lu, T. Wu, Q. Yuan, H. Wang, H. Wang, F. Ding, X. Xie, M. Jiang, *Nat. Commun.* **2015**, *6*, 6160.
[24] S. Caneva, R. S. Weatherup, B. C. Bayer, B. Brennan, S. J. Spencer, K. Mingard, A. Cabrero-Vilatela, C. Baehtz, A. J. Pollard, S. Hofmann, *Nano Lett.* **2015**, *15*, 1867.
[25] X. X. Yang, Z. X. Guan, M. Zeng, J. K. Wei, W. L. Wang, X. D. Bai, *Small* **2013**, *9*, 1353.
[26] H. L. Wang, X. W. Zhang, J. H. Meng, Z. G. Yin, X. Liu, Y. J. Zhao, L. Q. Zhang, *Small* **2015**, *11*, 1542.
[27] Y. Liu, S. Bhowmick, B. I. Yakobson, *Nano Lett.* **2011**, *11*, 3113.
[28] V. I. Artyukhov, Y. Hao, R. S. Ruoff, B. I. Yakobson, *Phys. Rev. Lett.* **2015**, *114*, 115502.
[29] H. Wang, G. Wang, P. Bao, S. Yang, W. Zhu, X. Xie, W. J. Zhang, *J. Am. Chem. Soc.* **2012**, *134*, 3627.
[30] A. Mohsin, L. Liu, P. Liu, W. Deng, I. N. Ivanov, G. Li, O. E. Dyck, G. Duscher, J. R. Dunlap, K. Xiao, G. Gu, *ACS Nano* **2013**, *7*, 8924.
[31] R. V. Gorbachev, I. Riaz, R. R. Nair, R. Jalil, L. Britnell, B. D. Belle, E. W. Hill, K. S. Novoselov, K. Watanabe, T. Taniguchi, A. K. Geim, P. Blake, *Small* **2011**, *7*, 465.
[32] L. F. Wang, B. Wu, L. L. Jiang, J. S. Chen, Y. T. Li, W. Guo, P. A. Hu, Y. Q. Liu, *Adv. Mater.* **2015**, *27*, 4858.
[33] A. C. Ferrari, J. C. Meyer, V. Scardaci, C. Casiraghi, M. Lazzeri, F. Mauri, S. Piscanec, D. Jiang, K. S. Novoselov, S. Roth, A. K. Geim, *Phys. Rev. Lett.* **2006**, *97*, 187401.
[34] K. S. Novoselov, A. K. Geim, S. V. Morozov, D. Jiang, Y. Zhang, S. V. Dubonos, I. V. Grigorieva, A. A. Firsov, *Science* **2004**, *306*, 666.
[35] W. Auwärter, H. U. Suter, H. Sachdev, T. Greber, *Chem. Mater.* **2004**, *16*, 343.
[36] R. Geick, C. H. Perry, G. Rupprecht, *Phys. Rev.* **1966**, *146*, 543.
[37] T. H. Yuzuriha, D. W. Hess, *Thin Solid Films* **1986**, *140*, 199.
[38] K. Watanabe, T. Taniguchi, H. Kanda, *Nat. Mater.* **2004**, *3*, 404.
[39] C. H. Zhang, L. Fu, S. L. Zhao, Y. Zhou, H. L. Peng, Z. F. Liu, *Adv. Mater.* **2014**, *26*, 1776.
[40] R. Y. Tay, X. Wang, S. H. Tsang, G. C. Loh, R. S. Singh, H. Li, G. Mallick, E. H. T. Teo, *J. Mater. Chem. C* **2014**, *2*, 1650.
[41] S. Joshi, D. Ecija, R. Koitz, M. Iannuzzi, A. P. Seitsonen, J. Hutter, H. Sachdev, S. Vijayaraghavan, F. Bischoff, K. Seufert, J. V. Barth, W. Auwärter, *Nano Lett.* **2012**, *12*, 5821.
[42] H. Kim, C. Mattevi, M. R. Calvo, J. C. Oberg, L. Artiglia, S. Agnoli, C. F. Hirjibehedin, M. Chhowalla, E. Saiz, *ACS Nano* **2012**, *6*, 3614.
[43] M. Sajjad, W. M. Jadwisienczak, P. Feng, *Nanoscale* **2014**, *6*, 4577.